

CANCOM2024 – CANADIAN INTERNATIONAL CONFERENCE ON COMPOSITE MATERIALS
**INTEGRATION OF INFRARED THERMOGRAPHY AND DIC FOR
DAMAGE CHARACTERIZATION IN NON-CRIMP FABRIC
REINFORCED POLYMER MATRIX COMPOSITES**

Shi, E.L.^{1*}, Qazi, H¹, Montesano, J¹

¹ Composites Research Group, Department of Mechanical & Mechatronics Engineering, University of Waterloo, Waterloo, Canada

* Corresponding author (erli.shi@uwaterloo.ca)

Keywords: *multiscale damage characterization ; digital image correlation ; infrared thermography*

ABSTRACT

A multiscale non-destructive evaluation approach combining in-situ digital image correlation and infrared thermography was used to characterize damage initiation and progression in non-crimp fabric glass fiber/epoxy composite laminates. Preliminary tests were conducted on standard width $[90]_4$ and $[0/90]_s$ rectangular specimens as well as open-hole $[0/90]_s$ specimens to establish the optimum test setup parameters for capturing local damage mechanisms. Subsequently, the same setup was used to perform quasi-static tensile tests on reduced width rectangular cross-ply specimens to capture damage evolution using digital image correlation and infrared thermography. The integrated non-destructive evaluation approach was capable of identifying the types of damage mechanism and their locations in-situ and in real time, including 90° ply cracks, 0° ply splitting cracks, and localized delamination, as well as damage evolution.

1 Introduction

The use of fiber reinforced polymeric (FRP) composite materials have become more prevalent in different engineering applications due to their excellent mechanical properties and significant weight benefits. This is evident in modern commercial transport aircraft like the Airbus 350 and the Boeing 787, where the airframe structure comprises over 50% composite materials by weight [1],[2]. In the automotive industry, due to the strict regulations legislated in different countries aiming to reduce CO₂ emissions and improve fuel efficiency for passenger vehicles [3]-[5], FRP composites are being integrated into body-in-white (BIW) structures, such as for BMW 2022 iX [6]. Despite the considerable advantages of using FRP composites, the complex hierarchical nature of damage in these materials makes it challenging to accurately characterize the damage evolution process and predict failure [7]. A thorough understanding of damage and failure mechanisms is important to improve the damage tolerance and integrity of composite structures. Non-destructive evaluation (NDE) techniques have been used to detect, identify, and locate damage, as well as evaluate damage evolution.

Digital image correlation (DIC) is a valuable in-situ NDE technique that enables the calculation of strain contours from surface displacements on FRP composites, which can be correlated with damage events [8],[9]. However, the application of this technique is restricted to detecting surface defects, and the accuracy is sensitive to the quality of the applied surface speckle pattern, the resolution of the optical cameras, the intensity of lighting used, and the parameters chosen to calculate strain contours. Infrared thermography (IRT), on the other hand, is a non-contact technique that can be used to continuously monitor damage development in-situ in FRP composites. It involves

CANCOM2024 – CANADIAN INTERNATIONAL CONFERENCE ON COMPOSITE MATERIALS

using an infrared (IR) camera to provide time-dependent contour maps of material surface temperature, resulting from energy release during damage initiation and propagation events. Several studies have successfully employed this technique to monitor damage development in FRP composites [10],[11]. However, the main drawbacks of IRT are that it may not always be able to detect small-scale damage due to the limited pixel resolution of the IR camera and the camera is sensitive to the surrounding environment. Also, damage in the internal layers of thick laminates may not be detectable by an IR camera since the associated heat releases may dissipate before reaching the surface.

The objective of this study is to integrate IRT and DIC as a combined NDE approach to effectively monitor damage evolution in non-crimp fabric glass fiber/epoxy composite laminates in-situ and in real time.

2 Material and Experimental Details

2.1 Material and manufacturing process

The material used in this study consisted of a unidirectional (UD) glass fiber non-crimp fabric (NCF) embedded within a thermoset epoxy resin. The UD-NCF (Saertex Group, Germany) comprised 3.42 mm wide NEG 2026 glass fiber tows in the 0° (longitudinal) direction and sparsely distributed supporting glass fiber yarns oriented in the 90° (transverse) direction, with linear densities of 2400 tex and 275 tex respectively (Fig. 1). Axially knitted polyester yarns with a linear density of 110 dtex in a tricot pattern were utilized to stitch and align the 0° glass fiber tows. Consequently, the NCF had a total areal density of 943 g/m². The commercially available liquid Pro-set® epoxy resin (Gougeon Brothers, USA) was used in conjunction with an amide hardener (Pro-set® INF-211) in a weight ratio of 100:27.4, as recommended by the manufacturer. This material system was kept constant throughout all tests performed.

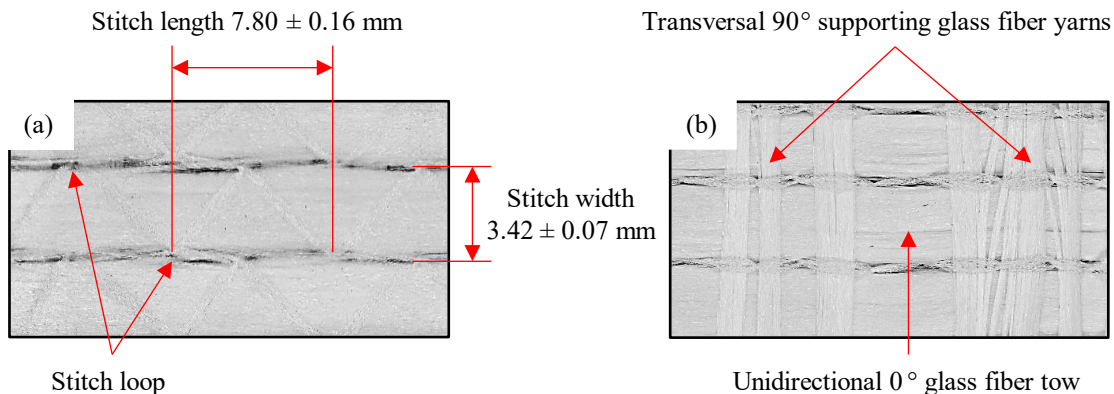


Fig. 1. Architecture of UD-NCF glass fiber layer: (a) top surface; (b) bottom surface[12].

A customized vacuum infusion process with a lower aluminum mold and vacuum bag was employed to fabricate flat composite panels consisting of 4 layers of UD-NCF with a stacking sequence of [90]₄ or [0/90]₅. The panels were subjected to a two-step curing process: 24 hours at room temperature followed by 8 hours at 82°C in a convection oven. The fiber volume fraction (V_f) of the panels was measured optically from cross-sectional samples using an opto-digital microscope (VHX-5000, Keyence) and found to be approximately 48%. Test specimens were cut from the panels using an abrasive waterjet cutting machine. Aluminum end tabs were adhesively bonded to all specimens to minimize the risk of premature end tab induced failure.

CANCOM2024 – CANADIAN INTERNATIONAL CONFERENCE ON COMPOSITE MATERIALS

2.2 Experimental procedures

All quasi-static tensile tests were conducted on a servo-electric Shimadzu test frame equipped with a +/-50 kN capacity load cell and hydraulic grips. Preliminary tests were performed on four standard-width rectangular specimens (25mm width) and five open hole specimens (hole diameter of 4.2 mm) with different stacking sequences under various displacement-controlled rates, ranging from 1mm/min to 2mm/min. These preliminary tests aimed to determine the minimum load required for damage initiation, consistently capture damage propagation, determine the optimum set-up parameters, and validate the developed NDE technique (refer to Fig. 2 for captured thermographic images). A reduced-width $[0/90]_s$ rectangular specimen in accordance with ASTM 3039 [13] (15mm width x 275mm length) loaded at a displacement rate of 1mm/min was chosen in this study to ensure onset of damage at a lower applied load and potentially reduce the rate of damage propagation, enabling the characterization of damage. A total of three tests were performed using the reduced width specimens, which showed consistent results.

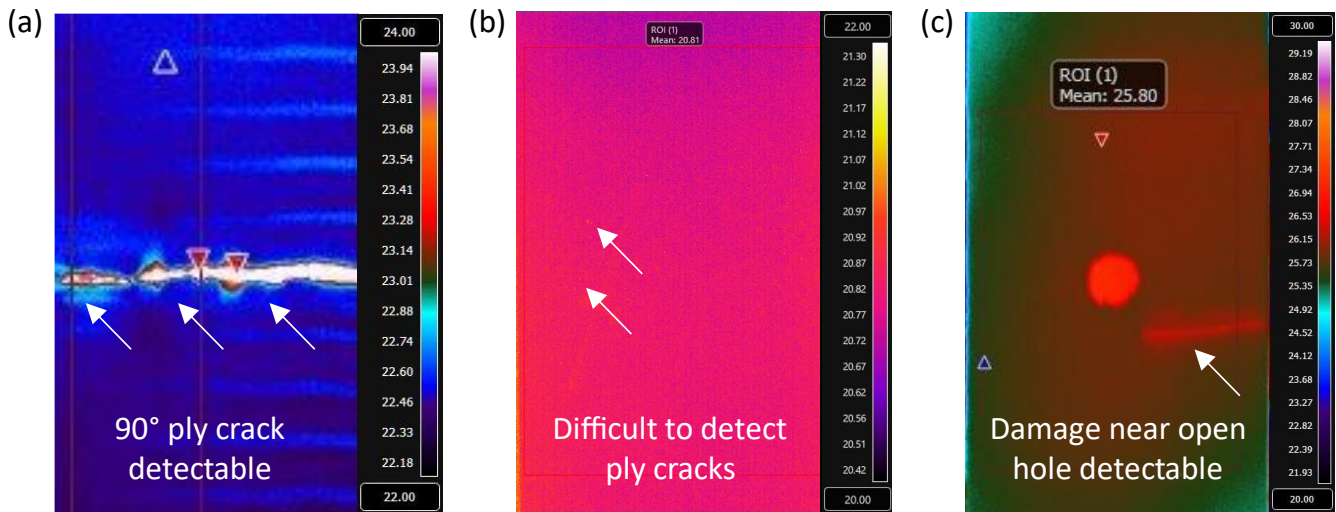


Fig. 2. Examples of thermographic images captured during preliminary test (displacement rate specified): (a) $[90]_4$ standard-width rectangular specimen (1mm/min); (b) $[0/90]_s$ standard-width rectangular specimen (2mm/min); (c) $[0/90]_s$ standard-width open-hole specimen (1mm/min).

A 5MP resolution digital camera was used on the mold side of the specimen to capture images at different applied displacements at a frame rate of 5Hz (Fig. 3a). The region of interest (ROI) was located at the center of the specimen gauge length and was finely speckle patterned with black and white spray paint. VIC-2D software was employed to determine the strain and displacement fields, which could be correlated to damage events. A subset size of 29 pixels, step size of 7 pixels, and filter size of 12 were used to calculate the strain maps within the ROI, while a virtual extensometer with a length of 20 mm was used to evaluate the average strain for stress-strain plots.

The FLIR A8581 IR camera with a pixel resolution of 1280 x 1024 and a temperature sensitivity of <25 mK was positioned on the opposite side of the specimen to monitor the surface temperature variations during testing (Fig. 3b), which could be correlated to damage events. FLIR Research Studio was used to postprocess the thermographic videos. To maximize heat emissivity and better capture thermal radiation, several approaches were employed according to the results from the preliminary tests: 1) a black background screen was used; 2) the specimen side facing the camera was sprayed with a black matte paint; 3) a precision optics was used to zoom in the field of view

CANCOM2024 – CANADIAN INTERNATIONAL CONFERENCE ON COMPOSITE MATERIALS

(FOV), and the FOV was narrowed so that only ROI of the specimen was displayed; 4) a maximum frame rate of 100Hz was employed during the testing to capture damage propagation.

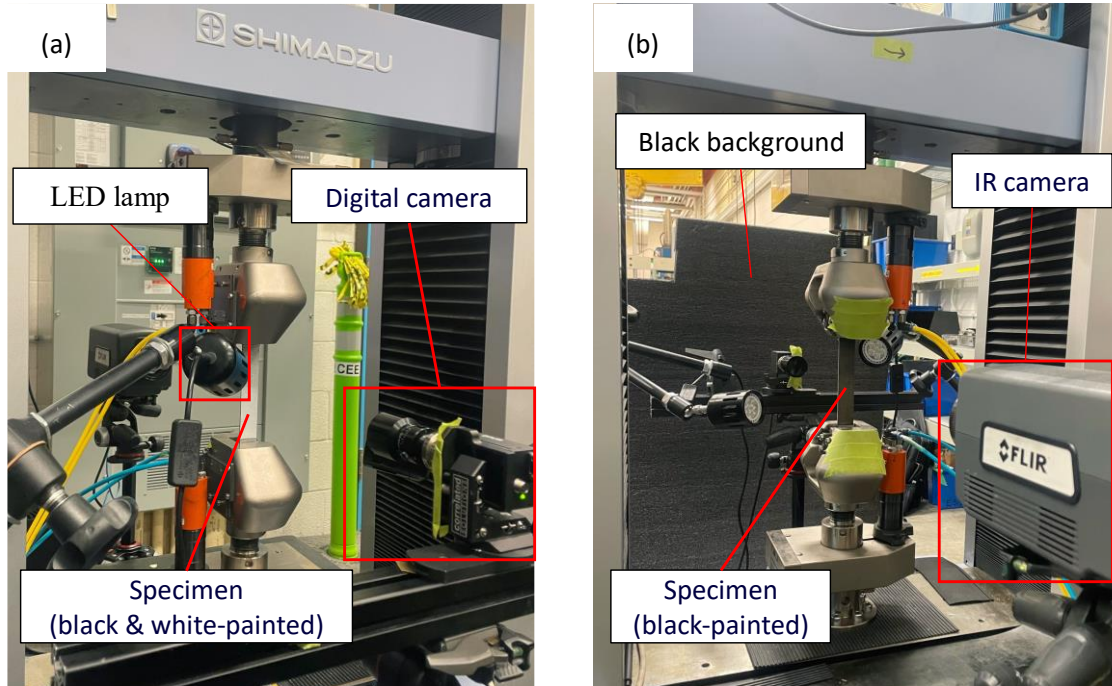


Fig. 3. Test set-up: (a) front view; (b) back view.

3 Results and Discussion

3.1 Damage characterization using DIC

Fig. 4 shows the material stress-strain response and strain contour maps at indicated strain levels in a sequential manner. The specimen exhibited a bi-linear stress strain response with a transition at ~ 0.006 strain. With further increase of the load, no evidence of plastic deformation was observed up to failure at ~ 0.030 strain. The damage evolution was also examined from the surface strain development. 90° fiber tow cracks were first observed at several locations along the specimen length at 0.006 strain (Fig. 4.1), which correlated well with the knee point observed in the stress-strain curves. A local maximum strain of 0.012 was observed at the cracked regions near the specimen edge. At ~ 0.010 strain (Fig. 4.2), 90° fiber tow cracks tended to propagate along the fiber direction across the entire width of the specimen. With further increase of the load (~ 0.023 strain, Fig. 4.3), additional 90° fiber tow cracks developed, and crack saturation was reached where crack spacing was uniformly distributed along the specimen length. A detailed illustration of a single crack propagation (a \rightarrow b \rightarrow c) during this stage further validated the initiation location of 90° fiber tow cracks. The maximum local strain was ~ 0.072 and there was no indication of other damage modes, such as 0° fiber tow cracks and large-scale delamination. The strain contour did not change significantly prior to the final failure of the specimen (~ 0.030 strain, Fig. 4.4).

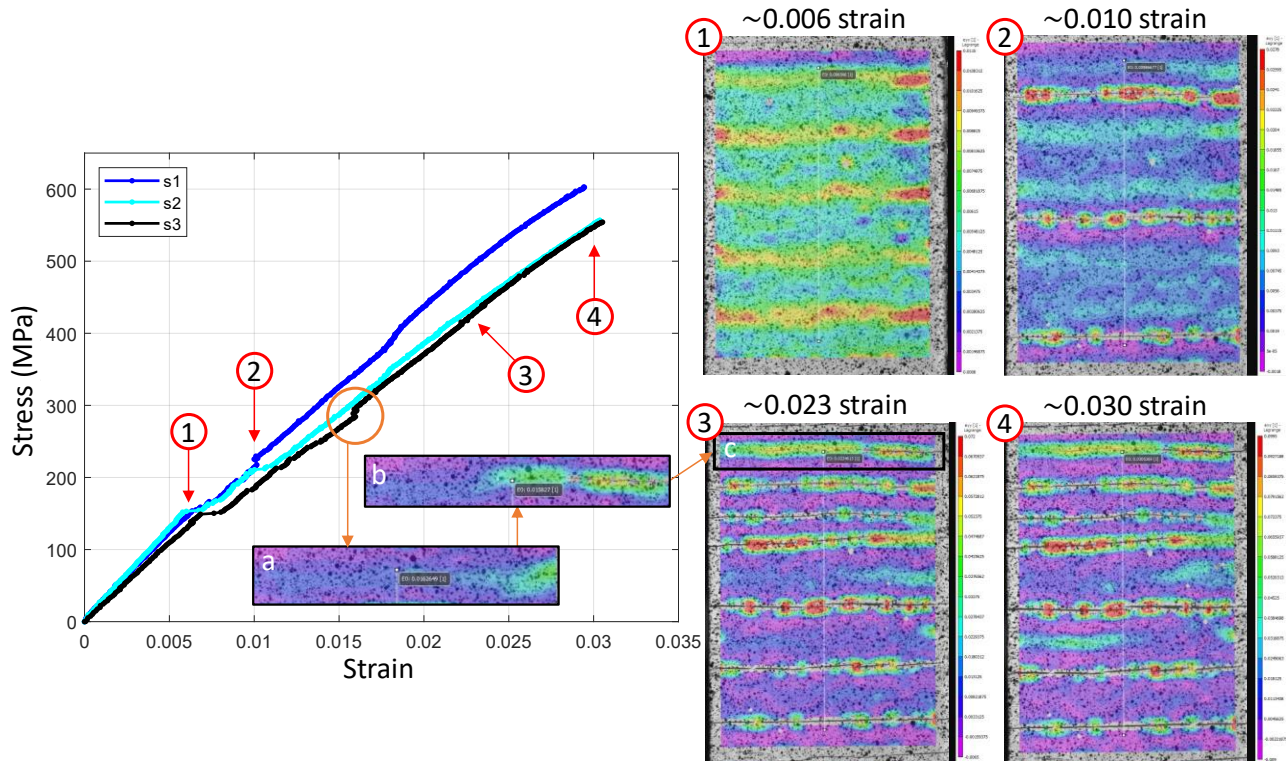


Fig. 4. Stress-strain response and damage characterization using DIC for a reduced width $[0/90]_s$ specimen.

3.2 Damage characterization using IRT

Fig. 5 shows the damage evolution process captured using IR thermography for the same specimen. The first individual 90° fiber tow crack was observed at a much lower strain of ~ 0.004 (Fig. 5a), which did not cause a kink in the stress-strain plot (Fig. 4) or a significant change in the secant modulus. The onset of the first individual 90° fiber tow crack may have been a result of localized manufacturing defects (e.g., voids). Moreover, the temperature variation due to crack initiation at the inner 90° fiber layers was less than 0.5°C compared to the undamaged region. As loading increased until ~ 0.006 strain (Fig. 5b), multiple 90° fiber tow cracks were observed at different locations along the specimen length, corresponding to the significant drop of the load (Fig. 4). This observation also correlated well with the results obtained using DIC. With further increase of the load prior to failure, ~ 0.030 strain (Fig. 5c), more damage modes were observed, such as multiple localized delamination cracks propagating along the 90° fiber tow peripherals in the longitudinal direction and 0° fiber tow splitting cracks. These critical damage modes could interact with each other, leading to the final failure of the specimen at ~ 0.031 strain (Fig. 5d).

Although same specimen was used to compare the damage evolution process using DIC and IRT, the contour maps of strain and temperature were different (i.e., Fig. 4.1 versus Fig. 5b at ~ 0.006 strain). Several possible reasons could cause this discrepancy. First, the digital and IR cameras were facing opposite sides of the specimen and the development of damage may have been distinct among different fiber layers. Fig. 6 shows the microscopic results of 90° fiber tow cracks developed at different layers by Shi et al. [12]. Two damage events were observed: 1) cracks propagated within their fiber tow in the same layer (Fig. 6a); 2) cracks coalesce between fiber tows in adjacent 90° fiber layers (Fig. 6b). Second, DIC allowed for the calculation of strain contours from specimen surface displacement, while IRT was able to capture the dissipated heat resulting from the initiation and propagation of damage even in

CANCOM2024 – CANADIAN INTERNATIONAL CONFERENCE ON COMPOSITE MATERIALS

subsurface areas. Third, a cumulative damage evolution process was obtained using DIC, while passive IRT enabled the in-situ monitoring of damage under the applied stress.

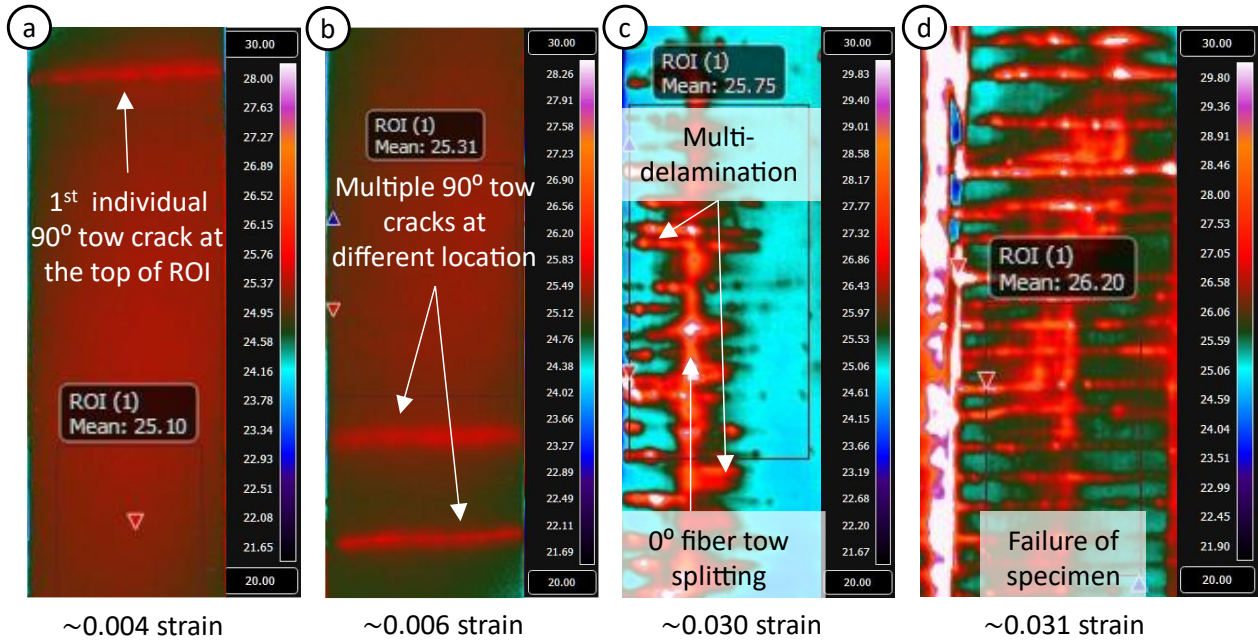


Fig. 5. Damage characterization using IRT at different applied stress for a reduced width [0/90]_s specimen.

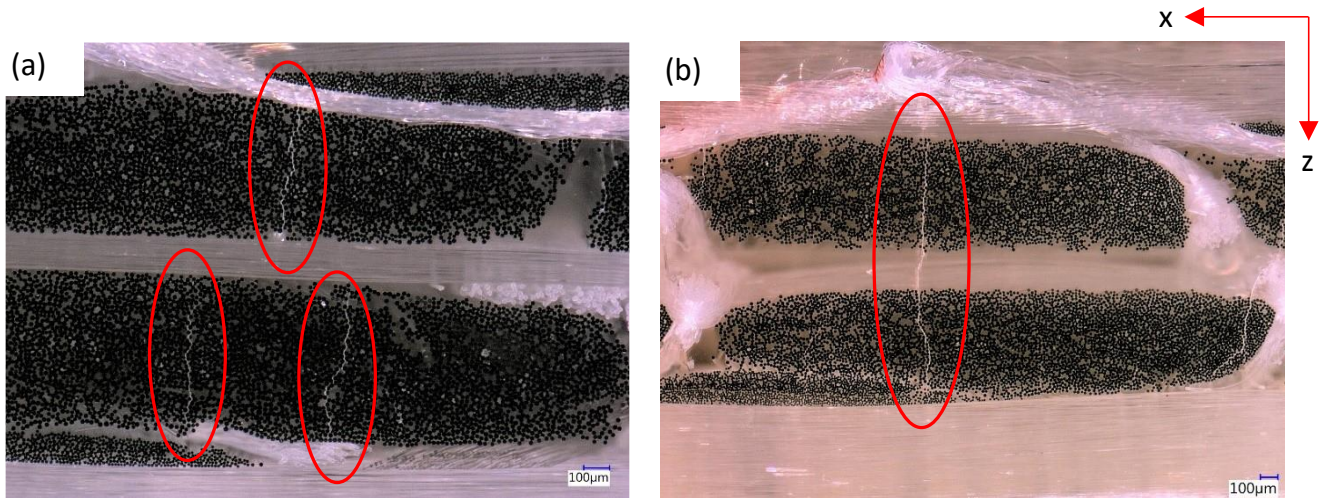


Fig. 6. Microscopic observation of 90° fiber tow cracks a) at different 90° fiber layers; b) across adjacent 90° fiber layers [12].

4 Conclusions

An integrated NDE technique combining DIC and IRT was employed in this study to characterize the damage evolution process of a cross-ply UD-NCF glass fiber/thermoset epoxy composite material under quasi-static tensile loading. Results demonstrated that both DIC and IRT were able to capture damage evolution based on surface strain maps and temperature variations respectively. IRT allowed for capturing more damage modes in-situ and in real time such as multiple localized delamination cracks and 0° fiber tow splitting cracks, while DIC enabled the cumulative monitoring of damage providing insights of the severity of damage in the specimen. Therefore, the developed NDE setup is useful for an in-situ identification of the types and locations of damage as well as a detailed chronology of the damage events for the studied material. Future investigation will center on broadening the application of this integrated technique to evaluate the fracture toughness and damage evolution in the fracture process zone for NCF composites.

5 References

- [1] L. Blumenfeld. "Flight airworthiness support technology—special edition A350XWB". Airbus Technical Magazine, June 2013.
- [2] J. Hale. "Boeing 787 from the ground up". AERO magazine. Q4 2006. [Online]. Available: http://www.lb.boeing.com/commercial/aeromagazine/articles/qtr_4_06/article_04_2.html [Accessed: 05/15/2024].
- [3] U. D. M.Ghosh. "The road ahead, national highway traffic safety administration, report". 2016.
- [4] S. Mccarthy. "Canada to copy Obama's fuel efficiency rules". The Globe and Mail, Aug. 2012. [Online]. Available: <https://www.theglobeandmail.com/report-on-business/industry-news/energy-and-resources/canada-to-copy-obamas-fuel-efficiency-rules/article4508608/> [Accessed: 05/15/2024].
- [5] D. Popp. "Fit for 55: zero CO2 emissions for new cars and vans in 2035". European Parliament, Feb 2023. [Online]. Available: <https://www.europarl.europa.eu/news/en/press-room/20230210IPR74715/fit-for-55-zero-co2-emissions-for-new-cars-and-vans-in-2035> [Accessed: 05/15/2024].
- [6] H. Mason. "BMW rolls out multi-material carbon cage with 2022 iX vehicle line". Dec. 2021. [Online]. Available: <https://www.compositesworld.com/articles/bmw-rolls-out-multi-material-carbon-cage-with-2022-ix-vehicle-line> [Accessed: 05/15/2024].
- [7] R. Talreja and C. V. Singh. "Damage and failure of composite materials". Cambridge University Press. 2012.
- [8] M. Tekieli, S. De Santis, G. de Felice, A. Kwiecień, and F. Roscini. "Application of Digital Image Correlation to composite reinforcements testing", *Composite Structures*, vol. 160, pp. 670–688, Jan. 2017.
- [9] M. Wang et al. "Fatigue damage monitoring of composite laminates based on acoustic emission and digital image correlation techniques". *Composite Structures*, vol. 321, p. 117239, Oct. 2023.
- [10] J. Montesano, H. Bougherara, and Z. Fawaz. "Application of infrared thermography for the characterization of damage in braided carbon fiber reinforced polymer matrix composites". *Composites Part B: Engineering*, vol. 60, pp. 137–143, Apr. 2014.
- [11] L.Toubal, M. Karama, and B. Lorrain. "Damage evolution and infrared thermography in woven composite laminates under fatigue loading". *International Journal of Fatigue*, vol. 28, no. 12, pp. 1867–1872, Dec. 2006.
- [12] E. Shi, J. Montesano. "Application of digital imaging technique in damage characterization of non-crimp fabric reinforced reactive thermoplastic composite at low temperature". *unpublished*.
- [13] ASTM D3039-17. "Standard test method for tensile properties of polymer matrix composite materials". *ASTM Int*, 2017.